EKF Estimation of Stride Width from Individual IMU-based Foot Trajectory Estimates

Michael V Potter, Kaiwen Liu, Mert Selamet, Giridharan Kumaravelu

Abstract— **Inertial measurement units are an increasingly attractive option for measuring human kinematics in naturalistic environments. Zero-velocity update (ZUPT) based foot trajectory estimates have been demonstrated to yield accurate estimates of individual foot stride metrics; however, there is an absence of literature establishing techniques to fuse individual foot trajectories to obtain estimates of stride parameters that rely on knowing the positions of both feet (e.g. stride width, base of support). In this project, an Extended Kalman Filter was developed to fuse individual foot trajectory estimates. These were calculated using position estimates obtained from a well-validated ZUPT-based algorithm and range measurements between the legs obtained from an ultrasonic sensor. The algorithm was validated and demonstrated accurate estimation of stride width during normal human walking with average error less than** 15%**.**

I. INTRODUCTION

The ability to measure human kinematics is essential for a broad range of research tasks including monitoring aging populations and improving athletic and warfighter performance. Today, the gold standard method for measuring human kinematics uses optical motion capture systems. However, use of these systems often constrains studies to traditional laboratory environments with limited capture volumes and where human kinematics are known to differ from naturalistic environments [2][3][4]. For this and many other reasons, miniature inertial measurement units (IMUs) are an increasingly attractive way to measure human kinematics outside of traditional laboratory environments [5][6][7]. Unfortunately, when seeking to obtain position information from IMUs, drift caused by integrating sensor noise can cause significant error if not appropriately corrected for [8]. Thus, many algorithms seeking to derive position information from IMUs must take advantage of known constraints to reduce errors caused by drift. In the context of biomechanics, one example of such a type of algorithm is zero-velocity update (ZUPT) algorithms developed to compute full 3-dimensional foot trajectory information from foot-mounted IMUs. These ZUPT algorithms take advantage of the fact that the foot reaches near zero-velocity during each stance phase of human walking or running. Thus, drift can be greatly reduced by correcting calculated velocity information (obtained from integrating the IMU's accelerometer data) by forcing the calculated velocity to be zero at each identified zero-velocity point. These algorithms also typically use a Kalman filter to help reduce error in the tilt angle of the foot. While these algorithms have demonstrated good accuracy for determining individual stride metrics (e.g. stride time, stride speed, foot clearance, stride length, etc.)[9][1], there is a lack of literature demonstrating methods for combining individual foot trajectory estimates to obtain other desired metrics such as stride width. Even if the starting positions of the two feet are exactly known, the challenge still remains since each foots calculated trajectory will have drift in heading angle. Knowledge of the relative position between the sensors could significantly reduce such heading drift and could also be valuable for obtaining accurate kinematic measures involving the position of both feet. Additionally, this could provide a solid basis for obtaining accurate full lower body kinematics with additional IMUs on the shanks and thighs. The goal of this project is to demonstrate the potential to use information about the relative position of two foot-mounted IMUs to fuse individual foot-trajectory estimates obtained from a ZUPT-based foot trajectory algorithm.

II. METHODS

A ZUPT-based foot trajectory algorithm similar to that described in [1] was used to estimate individual trajectories for the right and left feet from foot-mounted IMUs. Because this algorithm already uses an Extended Kalman Filter (EKF) to correct error in foot tilt estimation, there is very little drift in foot height estimation during walking. Thus, for this project, it is assumed the foot height estimation is accurate. As a result, an EKF is formulated only to correct error in the relative position of each foot with respect to each other in the horizontal plane. The following subsections describe in greater detail the EKF model formulation.

A. Notation

Correct designation of reference frames for positions, control inputs, and measurements is critical to appropriate implementation of the EKF algorithm described in this paper. As described at the beginning of this section (II), this project assumes estimates of foot height obtained from ZUPT-based foot trajectory algorithms to be accurate in walking. Therefore, the EKF problem presented here becomes a planar one. The variables x and y will hereafter denote the x and y positions while θ will denote a stride's heading angle. Additionally, changes in x, y, and θ will be denoted as Δx, Δy, and $\Delta\theta$ respectively. Superscripts will be used to denote the reference frame of the positions or their derivatives, with W denoting an inertial frame common to all estimates, M denoting the reference frame of the M^{th} right stride, and N denoting the reference frame of the N^{th} left stride. Subscripts R and L are used to clarify whether a variable pertains to the right or left foot respectively. Finally, subscripts t and $t-1$ denote an estimate pertaining to the current and previous

time steps respectively. Any other notation appearing in this text will be described as needed.

B. Control Input

Because raw outputs of ZUPT-based foot trajectory algorithms yield position estimates in an arbitrary world frame, they are not suitable as direct inputs into the traditional EKF framework. However, these individual trajectory estimates can be easily processed to make them useful as control inputs in the EKF framework. For the right foot trajectory, individual strides are first designated as starting at one zero-velocity update point and ending at the next zero-velocity update point. The overall heading angle of each stride, θ_R^W, is then calculated as the angle in the horizontal plane between the positive x-axis of the estimate's arbitrary world frame and the vector from the beginning to the end of the M^{th} right stride. Each stride is then assigned its own reference frame with the angle from the world frame and the stride frame being equal to the stride's overall heading angle as seen in Fig. 1. For the entire right trajectory, Δx_R^M and Δy_R^M are then calculated between each sample as the change in x and y estimates respectively, resolved in the current stride's reference frame. Additionally, for samples identified as zero-velocity update points (between strides), $\Delta\theta$ is calculated as the difference in heading angle between strides $M-1$ and M. For all other samples, $\Delta\theta$ is assigned a value of zero. A similar process is used to compute these values for the left foot with a stride index of N instead of M. By computing Δx_R^M, Δy_R^M, Δx_L^N, Δy_L^N, $\Delta\theta_R^M$, and $\Delta\theta_L^N$ in this manner, these values can easily be integrated as control inputs into the EKF framework as described in Section II-D.

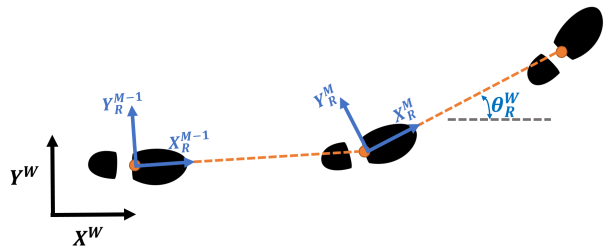

Fig. 1. Individual Stride Reference Frames

C. Measurements

In order to correct errors in the prediction model, a distance measurement device is attached to the left ankle pointing in the medial direction. Range measurements from this device can be used to establish two measurements, namely the distance between two feet perpendicular to the heading left foot z_1 and the distance between the feet parallel to the heading of the left foot z_2 as seen in Fig. 2.

Note that while z_1 is a direct output of the range sensor, z_2 is not an output of the range sensor. Instead, we take advantage of the fact the range sensor can only obtain a measurement to the right foot when the two feet are passing by each other (with z_2 approximately equal to zero). Thus we

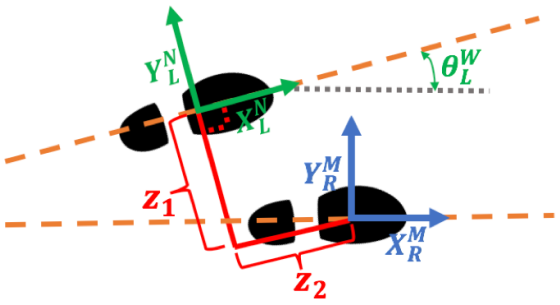

Fig. 2. Distance Measurement Model

generate a measurement of $z_2 = 0$ each time a measurement for z_1 is obtained from the range sensor. Employing this second measurement is a key to both increasing the rate of convergence of our EKF algorithm and obtaining accurate estimates of the relative position of the two feet. The formulation of the measurement model is described in Section II-D.

D. EKF Models

With the control inputs and measurements described in the previous two subsections, estimation of the planar position of the right and left foot can be formulated as a standard EKF problem. Because we are only concerned with correcting error in the foot position estimates in the horizontal plane, the estimated joint state of both feet can be fully described as a 6-dimensional vector, μ, containing the x and y positions of each foot in the world frame as well as each foot's heading angle, θ. Thus, the estimated joint state becomes:

$$\mu = [x_R^W, y_R^W, \theta_R^W, x_L^W, y_L^W, \theta_L^W]^T. \tag{1}$$

The control input at each time step, as described in Section II-B, can also be combined in one joint control vector, u:

$$u = [\Delta x_R^M, \Delta y_R^M, \Delta\theta_R^M, \Delta x_L^N, \Delta y_L^N, \Delta\theta_L^N]^T. \tag{2}$$

The motion model, or action model, yields the state transition probability of the state, $p(X_t|u_t, X_{t-1})$, where X_t is the current state, u_t is the current control input, and X_{t-1} is the previous state and explains the posterior distribution. This is estimated in the prediction step in the EKF. For our system, the predicted current state, $\overline{\mu_t}$, is calculated using Equation 3:

$$\overline{\mu_t} = \mu_{t-1} + \begin{bmatrix} \Delta x_R^M \cos(\theta_R^W + \Delta\theta_R^M) - \Delta y_R^M \sin(\theta_R^W + \Delta\theta_R^M) \\ \Delta y_R^M \cos(\theta_R^W + \Delta\theta_R^M) + \Delta x_R^M \sin(\theta_R^W + \Delta\theta_R^M) \\ \Delta\theta_R^M \\ \Delta x_L^N \cos(\theta_L^W + \Delta\theta_L^N) - \Delta y_L^N \sin(\theta_L^W + \Delta\theta_L^N) \\ \Delta y_L^N \cos(\theta_L^W + \Delta\theta_L^N) - \Delta x_L^N \sin(\theta_L^W + \Delta\theta_L^N) \\ \Delta\theta_L^N \end{bmatrix} \tag{3}$$

where μ_{t-1} is the estimate of the previous state and all other variables are as previously defined. Note that all state

variables (e.g. θ) in Equation 3 are from the previous time step while all control inputs are from the current time step.

Because the motion model is nonlinear, linearization is required to estimate the predicted covariance of the state. Thus, the Jacobians, G and V, of the action model with respect to the state and control input respectively are also calculated to find the predicted covariance, $\overline{\Sigma_t}$ from the covariance at the previous time step Σ_{t-1}:

$$\overline{\Sigma_t} = G\Sigma_{t-1}G^T + VRV^T, \tag{4}$$

where R is the control noise.

In the measurement model, the procedure for which sensor measurement to be generated are revealed. The probability is represented as $p(z_t|X_t)$ where z_t is the current measurement, which is a product of each measurement likelihood:

$$p(z_t|X_t) = \prod_{k=1}^{K} p(z_t^k|X_t), \tag{5}$$

where K is the number of measurements and z_t^k is a single measurement. This is formulated in the EKF update step. The model for the experiment is described in Equation 6:

$$\bar{z} = \begin{bmatrix} z_1 \\ z_2 \end{bmatrix} = \begin{bmatrix} (x_R^W - x_L^W)\sin\theta_L^W - (y_R^W - y_L^W)\cos\theta_L^W \\ (x_R^W - x_L^W)\cos\theta_L^W - (y_R^W - y_L^W)\sin\theta_L^W \end{bmatrix}, \tag{6}$$

where z_1 and z_2 are the distances indicated in Fig. 2. The Jacobian of the measurement model with respect to the state, H, is then calculated and what remains is the familiar EKF update step:

$$\begin{aligned} K_t &= \Sigma_t H^T (H\Sigma_t H + Q)^{-1} \\ \mu_t &= \bar{\mu}_t + K_t(z - \bar{z}) \\ \Sigma_t &= (I - K_t H)\overline{\Sigma_t} \end{aligned} \tag{7}$$

where Q is the measurement covariance, $\bar{z}$ is the predicted measurement, and Σ_t is the covariance of μ_t.

In the study presented in this paper, control inputs were received at a much higher rate (128 Hz) than measurements (approximately one per stride). Thus, after each prediction step, the update step was applied only if a measurement was available; otherwise, the next prediction step was made.

III. Validation of Algorithm

A simple experiment was conducted in order to validate the presented algorithm. This required the selection and implementation of a range measurement device capable of accurately measuring the distance between two feet at least once per stride during human walking. Additionally, a wearable IMU was selected to measure each foot's motion. The following subsections describe the hardware and experiment used for validation.

A. Hardware/Setup

The range sensor for this experiment needed to meet a few criteria. Firstly, the sensor must be affordable due to the budget of the project. Secondly, the sensor must have a high enough sampling rate to obtain at least one measurement of the distance between the two feet per stride. Thirdly, the sensor must be capable of accurately measuring distances between 10 and 100 cm (typical of stride widths in normal human gait). Finally, the distance sensor must provide measurement accuracy with about 1% uncertainties over these distances.

With these criteria, an ultrasonic sensor (HC-SR04) was selected due to a price of $2, measurement range of 2 - 400 cm, and a standard deviation of measurement error around 0.2 cm. The ultrasonic sensor was attached to a strap, allowing it to be mounted to the ankle as shown in Fig. 3. Additionally, an Arduino with an SD card shield was programmed to log distance measurements. This Arduino and a battery were mounted with the ultrasonic sensor to enable data collection without the subject being wired to a computer.

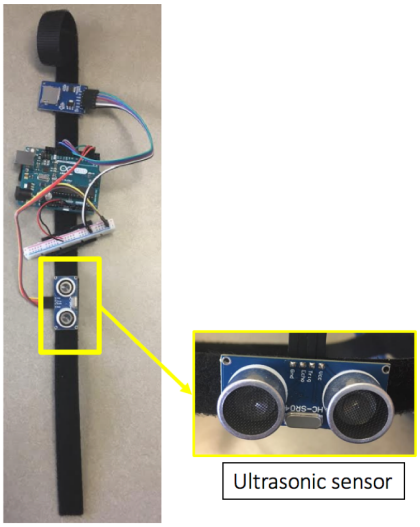

Fig. 3. Distance Measurement Device

A wearable IMU (APDM, OPAL, 128 Hz, ±200 g, ±2000 deg/s) was also attached to the instep of each foot. The overall setup of the sensors is shown in Fig. 4. Note that the distance measurement device will only have useful measurement when the two legs across each other in the side view. The sampling rate of the ultrasonic sensor was set to 30 Hz to maximize the number of strides for which a measurement is obtained while also avoiding degradation in accuracy. With this sampling rate, the device was able to capture a measurement on more than 80% of strides during a normal human walk.

B. Experimental Procedure

For the validation experiment, the IMUs and ultrasonic sensor were attached to the subject's feet/ankle. The subject was then asked to complete a straight line walk of approximately 50 meters, then take a 90 degree turn followed by another straight line walk of approximately 25 meters. During the straight line phases, the subject was asked to step on known markers (marked corners of 0.3m x 0.3m tiles) as shown in Fig. 5. This yields ground truth data that during double support phases (when both feet are on the ground)

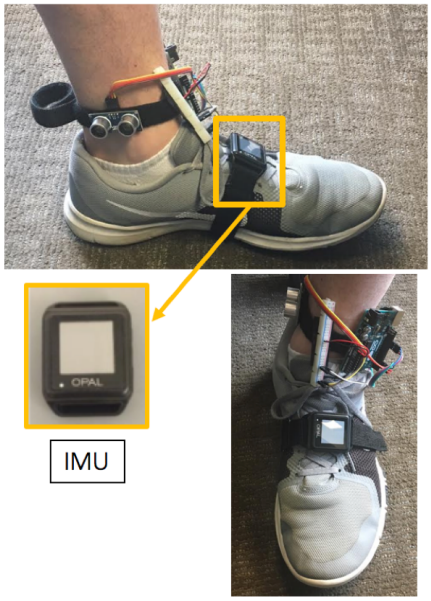

Fig. 4. Data Collection Setup

the stride width is 0.3 m and the distance between the feet parallel to the heading direction is 0.61 m.

Fig. 5. Experiment of Walking in a Hall Way

C. Data Processing

Data from the ultrasonic sensor were processed to yield distance measurements. All measurements greater than 0.50 meters were discarded since they were likely a result of errors or measurements objects other than the right leg. Additionally, any measurements taken during a turn were discarded because the measurement model proposed in Section II-D is not well suited for turning. Data obtained from each foot's IMU were processed using a ZUPT-based foot trajectory algorithm to obtain individual foot trajectory estimates and then further processed to yield control inputs as described in Section II. The IMUs used in this study are automatically synchronized; however, the range measurement data and IMU data were synchronized manually using known features in the raw IMU gyroscope data to identify mid-swing phases. Each valid range measurement was then assigned to the nearest time step in the IMU data and all other time steps in the IMU data were assigned no measurement. The EKF described in Section II-D was then used to estimate the combined trajectory of the right and left feet. Instances of double support were identified using the raw acceleration outputs of each IMU to identify heel strike and toe off instances for each foot. Finally, the estimated joint state of the right and left feet during these identified double support instances was then compared to ground truth estimates.

IV. Results and Discussion

Fig. 6 shows the individual horizontal foot trajectory estimates obtained from the ZUPT-based foot trajectory algorithm. Note that in this figure, the estimated trajectories for the right and left feet are obtained in different inertial reference frames. The ZUPT algorithm chooses to initialize the initial position as (0,0) and the first few strides to be generally in the positive x direction which is why both right and left foot trajectories appear to start in the same direction. However, each foot's trajectory estimate has no dependence on the other and thus no metric requiring knowledge of the relative position of the two feet can be estimated from these two independent trajectory estimates alone. It should be further noted that, even if relatively good initial estimation of the initial positions and heading angles of each foot are known, this figure shows that even small misalignments between each estimate's inertial frame will lead to the individual trajectories diverging from each other quickly.

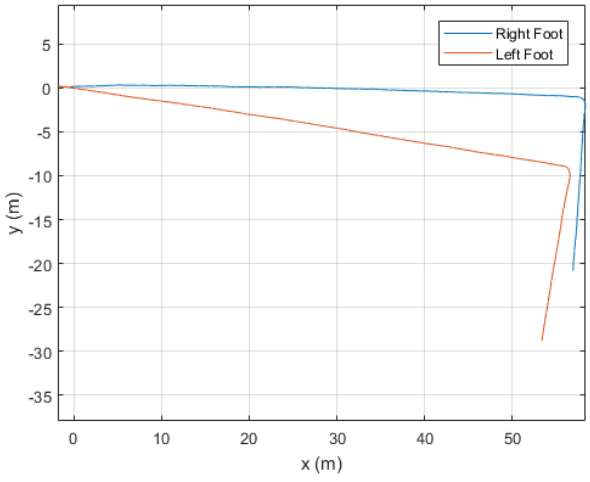

Fig. 6. ZUPT Output: Individual Foot Trajectories

The estimated foot trajectories using the EKF algorithm in II-D on the collected data are shown in Fig. 7. It can be seen in this figure that, unlike in Fig. 6, the right and

left foot trajectories do not drift apart during the entire trail. However, it is readily apparent that there are significant errors in the overall trajectory estimated using this method. This is observable in the large EKF update correction that can be seen after the turn. Deeper investigation into the cause of this larger correction (and many other more modest, but still noticeable corrections) showed that this is likely in part due to the noise parameters (especially R) used in this model. Because the control input for this EKF algorithm was derived from ZUPT-based foot trajectory estimates, rather than from the IMU data directly, it is difficult to accurately model the noise in these derived control inputs. Thus R was based on the accuracy of these position estimates as reported in the literature. It is likely though, that while these noise parameters are appropriate for straight line walking, they are not well suited for other tasks, such as turning.

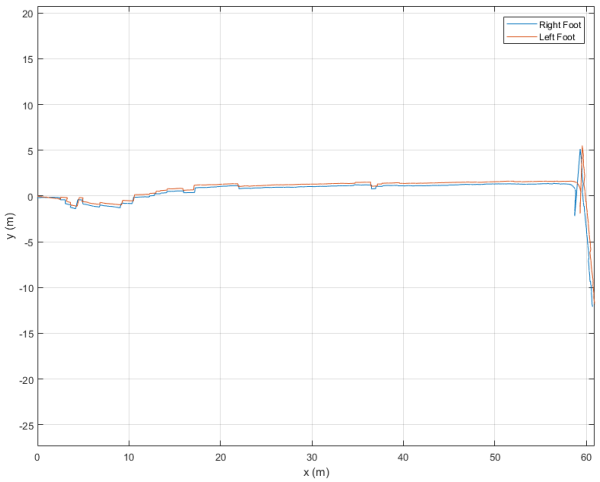

Fig. 7. EKF Output: Estimated Two-foot Trajectories

The experimental trial was split into three sections for better evaluation of the performance over time and with turning. All three sections are composed entirely of straight line walking since ground truth relative positions were not measured during the turning phase. The first section chosen is the first 28 meters of the trial with the second section the next 28 meters and the third section the remaining straight line walking after the turn. Trajectory estimates from these three sections are shown in Fig. 8. It can be seen that in the first section, relatively large corrections are frequently applied during measurement update steps. This causes the trajectory estimates to be very jagged, although the stride width seems to remain fairly consistent. These large corrections are likely a result of errors in estimating the initial state. During the first few update steps, the EKF harshly corrects the state because the measurements reveal error in the current state estimate. However, after a few update steps, much of this error is corrected. Thus, during the second section, there are much fewer large corrections during measurement update steps. This results in a fairly natural looking trajectory for most of the section while maintaining reasonable stride width estimates. In the third section, it is apparent that many of the measurement updates result in moderate trajectory corrections which yield a trajectory that looks somewhat jagged (although not as poor as in section 1). It should also be noted that careful inspection of this section will show that stride width estimation remains fairly accurate here, but the distance between the feet parallel to the heading direction has become very poor. This is likely a result of error accumulated during the turn. Even small errors in heading angle going into the turn can result in significant error in the estimated distance between the two feet parallel to the left foot's heading direction. The low sensor noise of the ultrasonic sensor allows error in the stride width accumulated over the turn to be corrected very quickly after only a couple update steps. However, there is much greater uncertainty in the z_2 "measurement" since it is only based on knowing the feet are approximately crossing each other when a range measurement is detected. This error could be reduced by improving the noise models as described in the previous paragraph. Additionally, better measurement sensors and/or better measurement models could allow for EKF update steps to be applied more often and even during turning. This could significantly reduce the drift observed during turning, likely leading to a lower likelihood that the algorithm applies such large corrections at the first update after a turn.

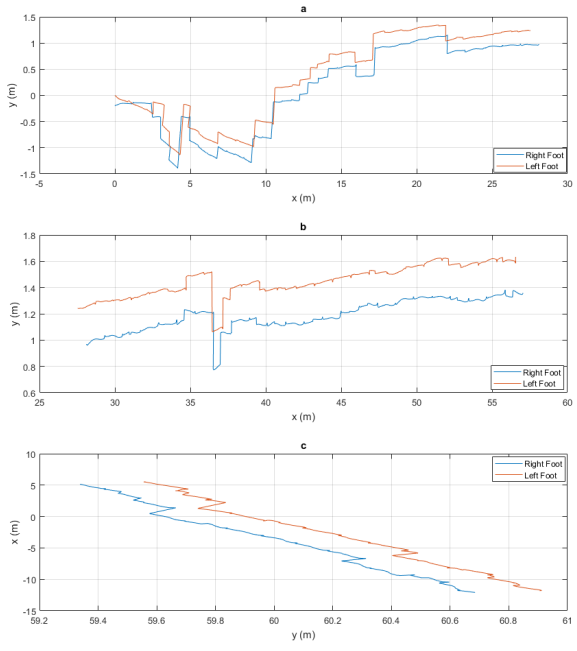

Fig. 8. Sectioned estimates of the foot trajectories: (a) Section 1: First 28 meters (b) Section 2: Second 28 meters (c) Section 3: Straight Walking after turn

The estimated stride width over time is plotted for all data points in the first and second sections combined and is shown

in Fig. 9. This figure also shows the standard deviation of the stride width over a moving window of the previous 500 data points. Because this was a controlled walking task that required the subject to maintain a consistent stride width, we would expect a low standard deviation. It is clear from this figure that during the first few strides, the estimated stride width has a very high standard deviation, however after only a few measurement updates to correct errors in estimating the initial state vector, the estimated stride width becomes very consistent as desired. This result suggests that stride width estimation using the method proposed in this paper may be inaccurate over the first few steps, but may become much more accurate and reliable over longer timescales of continuous walking.

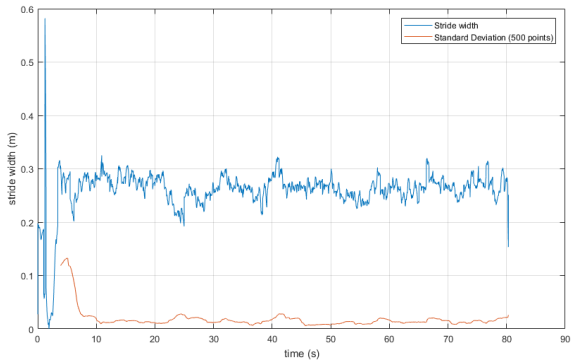

Fig. 9. Plot of the estimated stride width over time along with standard deviation calculated in a moving window of 500 data points

As described in Section III-C, periods of double support were used to obtain ground truth data of the relative positions of the right and left feet. The estimated stride width and distance between the feet parallel to the left foot's heading direction were calculated for each time step when double support occurred. These two estimates are essentially estimates of z_1 and z_2 as described in Fig. 2 respectively and thus are referred to as such in Table I. Table I shows the mean error and standard deviation of the error in estimated z_1 (stride width) and z_2 versus ground truth (0.30 m and 0.61 m respectively) for each of the three sections of straight walking. Note that the mean and standard deviation of the error in stride width estimates are very poor in the first section, but improve in the second section. Additionally, the accuracy of this stride width estimation remains fairly consistent from the second to third sections despite the turn. This suggests that although large EKF update corrections are observed after turning which severely degraded overall trajectory estimates, the EKF proposed in this paper retains reasonable accuracy for stride width estimation. In particular, comparing the mean stride width error found in Table I to the known ground truth stride width (0.30 m) reveals a mean error less than 15% for both the second and third sections. It should also be noted that some of the mean error could be contributed to other measurement uncertainty. Contributions to this uncertainty include the fact that the IMU estimated trajectories yield estimates of the positions of the IMUs (used as a proxy for the positions of the feet) through time and thus the state vectors are estimates of the IMU locations which are assumed to be nearly the foot locations. The ultrasonic sensor, however, is measuring the distance from the medial side of the left ankle to the medial side of the right leg. Thus a scalar offset was applied to measurement model to account for the medial-lateral distance from the left IMU to the ultrasonic sensor and from the medial side of the right ankle to the right IMU. Error in this measurement could result in a constant bias in error for stride width estimation. For this reason, the low standard deviation of stride width error in the second and third sections is even more encouraging than the relatively low mean error. Additionally, there is some uncertainty in the ground truth positions as well since the subject was asked to step on specific marker on the ground. Since both the mean and standard deviation of stride width error are within the uncertainties in ground truth positions and the measurement model's scalar offset as described, the results for stride width estimation accuracy are very encouraging and warrant further research. The mean and standard deviation of error in estimated z_2 also significantly improves from the first to the second section. However, the error in these estimates becomes very poor after the turn as demonstrated by the high standard deviation in the error. This could be a result of many of the challenges described earlier in this section including the control input noise model and the lack of measurement updates during the turning. Further work will need to be done to see if error in this parameter would be corrected again with sufficiently long straight walking following the turn (similar to the improvement in this parameter seen from the first to the second sections).

TABLE I

MEAN AND STANDARD DEVIATION OF z_1 AND z_2

Section	$\mu[z_1]$(m)	$\sigma[z_1]$ (m)	$\mu[z_2]$ (m)	$\sigma[z_2]$ (m)
Section 1	0.2461	0.0014	-0.2157	0.0032
Section 2	0.0437	0.0179	0.0480	0.0673
Section 3	0.0331	0.0184	0.0082	0.5542

V. CONCLUSIONS

Overall this project demonstrated great potential for implementing additional sensors to accurately combine individual IMU-based foot trajectory estimates. The primary goal of the project was to accurately estimate stride width from two individual foot trajectory estimates and a range measuring device. This goal was accomplished well with less than 15% mean error in stride width and approximately 6% standard deviation of stride width error. Both of these figures fall well within uncertainties of the ground truth data used and offsets applied to the measurement model. Thus, these results demonstrate the great potential of future work to further improve stride width estimates from minimal arrays of body worn sensors. Error in the distance between the right and left feet parallel to the left foot's heading direction showed

similar potential in straight line walking. However these estimates severely degraded after turning. Future work will need to reveal the full cause of these errors and methods to minimize them.

VI. FUTURE DIRECTIONS

This project demonstrated some of the vast potential to use additional body worn sensors to fuse individual IMU-based foot trajectory estimates. Future work could improve estimates of stride width by using better sensors to measure the relative positions of the feet. These sensors could include any combination of improved measurement accuracy, increased number of measurements per stride, or measurements suitable to be applied during turning, etc. Other work could include improving on the models presented in this work. For example, implementing an EKF as described in this paper but without a ZUPT-based foot trajectory algorithm. Thus, the control inputs would be the raw IMU signals themselves, allowing for much better modeling of the control input uncertainty which could lead to significantly improved estimates. In addition to improving stride width estimates by improving the models within the EKF framework, other future work should explore the use of other probabilistic estimation techniques such as unscented or particle filter. Additionally, smoothing techniques (as opposed to filtering) may prove valuable for improving accuracy, especially in applications where the entire trajectory is desired rather than the just the two measures z_1 (stride width) and z_2 (also important if base of support is to be estimated) focused on in this project.

While there are many things that can be done to improve the fusion of two foot trajectory estimates, these improvements could lead to even broader and more exciting applications. One such application is in obtaining full lower body kinematics with a minimal set of wearable sensors. Unlike the feet, other lower limbs are not subject to zero-velocity updates and thus it becomes much more challenging to reduce drift in their position and orientation estimates. However, successful fusion of individual foot trajectory estimates could form the base to close a lower body kinematic loop (from foot to shank to thigh to opposite thigh to opposite shank to opposite foot back to starting foot) that could unlock vast improvement in IMU based estimation techniques of lower body kinematic information (e.g. knee angle, pelvis tilt, etc.).

VII. OPEN SOURCE CODE

Our EKF algorithm is available for use as an open source MATLAB code at [10]. This is accompanied by a README file with instructions for implementing the code and a sample data set. You can also find additional information about this project including videos of our experiment and results on our website at [11].

REFERENCES

[1] L. Ojeda and J. Borenstein, Non-GPS Navigation for Security Personnel and First Responders, Journal of Navigation, vol. 60, no. 03, p. 391, Sep. 2007.

[2] J. H. Hollman, M. K. Watkins, A. C. Imhoff, C. E. Braun, K. A. Akervik, and D. K. Ness, A comparison of variability in spatiotemporal gait parameters between treadmill and overground walking conditions, Gait & Posture, vol. 43, pp. 204-209, 2016.

[3] M. Mckenna and P. E. Riches, A comparison of sprinting kinematics on two types of treadmill and over-ground, Scandinavian Journal of Medicine & Science in Sports, vol. 17, no. 6, pp. 649-655, Jan. 2007.

[4] L. V. Ojeda, J. R. Rebula, A. D. Kuo, and P. G. Adamczyk, Influence of contextual task constraints on preferred stride parameters and their variabilities during human walking, Medical Engineering & Physics, vol. 37, no. 10, pp. 929-936, 2015.

[5] N. Kitagawa and N. Ogihara, Estimation of foot trajectory during human walking by a wearable inertial measurement unit mounted to the foot, Gait & Posture, vol. 45, pp. 110-114, 2016.

[6] T. Seel, J. Raisch, and T. Schauer, IMU-Based Joint Angle Measurement for Gait Analysis, Sensors, vol. 14, no. 4, pp. 6891-6909, 2014.

[7] R. Vitali, S. Cain, R. Mcginnis, A. Zaferiou, L. Ojeda, S. Davidson, and N. Perkins, Method for Estimating Three-Dimensional Knee Rotations Using Two Inertial Measurement Units: Validation with a Coordinate Measurement Machine, Sensors, vol. 17, no. 9, p. 1970, 2017.

[8] D. H. Titterton and J. L. Weston, Strapdown inertial navigation technology. Stevenage: The Inst. of Engineering and Technology, 2009.

[9] A. Peruzzi, U. D. Croce, and A. Cereatti, Estimation of stride length in level walking using an inertial measurement unit attached to the foot: A validation of the zero velocity assumption during stance, Journal of Biomechanics, vol. 44, no. 10, pp. 1991-1994, 2011.

[10] https://gitlab.com/girikum/ekf-stridewidth.git

[11] https://foottrajresearch.weebly.com/